CIRCULATION ANALYSIS IN THE NORTHWEST INDIAN OCEAN USING ARGO FLOATS AND SURFACE DRIFTER OBSERVATIONS, AND SODA REANALYSIS OUTPUT

Sarah Stryker Vitale[1], Steven F DiMarco[2], Howard F Seidel[3], Zhankun Wang[4,5]

Affiliation address for all authors:
Department of Oceanography, Texas A&M University, College Station, TX 77843, USA

[1] Email: sarah.stryker@uconn.edu
Present address:
Center for Integrative Geosciences
University of Connecticut
354 Mansfield Road
Storrs, CT 06269

[2] Email: sdimarco@tamu.edu

[3] Email: hankseidel@yahoo.com

[4] Email: g.zhankunwang@gmail.com
Present address:
National Centers for Environmental Information, NOAA
Silver Spring, MD, 20910, USA
and
[5]Earth System Science Interdisciplinary Center
University of Maryland
College Park, MD 20740, USA

Highlights

- 1°x1°-resolution circulation patterns at surface, 1000, 1500 and 2000 m
- Great Whirl observed forming during Spring intermonsoon, lasting until Fall intermonsoon
- SODA reanalysis output and surface drifters velocity vectors have correlations of 0.71-0.93

Abstract

This study incorporates observations from Array of Real-time Geostrophic Oceanography (ARGO) floats and surface drifters to identify seasonal circulation patterns at the surface, 1000 m, 1500 m, and 2000 m in the northwest Indian Ocean, and quantify velocities associated with them. A skill comparison of the Simple Ocean Data Assimilation (SODA) reanalysis output was also performed to contribute to the understanding of the circulation dynamics in this region.

Subsurface currents were quantified and validated using the ARGO float data. Surface currents were identified using surface drifter data and compared to the subsurface observations to enhance our previous understanding of surface circulations. Quantified Southwest Monsoon surface currents include the Somali Current (v_{max} = 179.5 cm/s), the East Arabian Current (v_{max} = 52.3 cm/s), and the Southwest Monsoon Current (v_{max} = 51.2 cm/s). Northeastward flow along the Somali coast is also observed at 1000 m (v_{max} = 26.1 cm/s) and 1500 m (v_{max} = 12.7 cm/s). Currents associated with the Great Whirl are observed at the surface (v_{max} = 161.4 cm/s) and at 1000 m (v_{max} = 16.2 cm/s). In contrast to previous studies, both ARGO and surface drifter data show the Great Whirl can form as early as the boreal Spring intermonsoon, lasting until the boreal Fall intermonsoon. The Arabian Sea exhibits eastward/southeastward flow at the surface, 1000 m, 1500 m, and 2000 m. Quantified

Northeast Monsoon surface currents include the Somali Current (v_{max} = 97.3 cm/s), Northeast Monsoon Current (v_{max} = 30.0 cm/s), and the North Equatorial Current (v_{max} = 28.5 cm/s). Southwestward flow along the Somali coast extends as deep as 1500 m.

Point-by-point vector and scalar correlations of SODA output to ARGO and surface drifter data showed that surface SODA output and surface drifter data generally produced a strong correlation attributed to surface currents strongly controlled by the monsoons, while subsurface correlations of SODA output and ARGO were mostly insignificant due to variability associated with intermonsoonal transitions. SODA output produced overall smaller velocities than both observational datasets. Assimilating ARGO velocities into the SODA reanalysis could improve subsurface velocity assimilation, especially during the boreal fall and spring when ARGO observations suggest that flow is highly variable.

Keywords: Oceanic circulation, monsoons, current observations, surface drifters, ARGO

1. Introduction

The northwest Indian Ocean is a region of complex circulation and atmospheric influence (Schott et al., 2009), with near-surface circulation strongly influenced by the seasonal monsoon (Shi et al., 2000; McCreary and Kundu, 1989). Understanding the physical circulation dynamics in this region is critical, given its influence on seasonal rainfall (Izumo et al., 2008), hypoxia in the Arabian Sea (Morrison et al., 2005; McCreary et al., 2013) and Sea of Oman (Shi et al., 2000; Piontkovski and Al-Oufi, 2015), seasonal and annual plankton and fish biomass

variation (Smith and Madhupratap, 2005; Wang et al., 2014) and long-term climate variability (Schott et al., 2009).

1.1 Background

The study area is bounded by 0˚N-35˚N and 40˚E-80˚E, which includes the Sea of Oman, Arabian Sea, and the Gulf of Aden (Figure 1). Known surface currents in the northwest (NW) Indian Ocean during the northeast (NE) and southwest (SW) Monsoons are shown in Figure 1. There is substantial water exchange with the neighboring SW and NE Indian Oceans, which is also taken into account in this analysis. During the SW Monsoon, surface flow is generally to the east in the Arabian Sea. The Southwest Monsoon Current (SC) and East Arabian Current (EAC) flow to the northeast along the coasts of Somalia and Oman, respectively. In the SW Indian Ocean, the East African Coastal Current (EACC) (Schott and McCreary, 2001; Tomczak and Godfrey, 2013) flows northward along the east coast of Africa, north of Madagascar, extending toward the NW Indian Ocean. The structure of the EACC has been observed in DiMarco et al. (2002) as having a width around 200km and maximum subsurface velocities near 20 cm/s at 1000 m. The EACC splits after passing over the equator, with a portion of the current contributing to the Somali Current (Jensen, 1991), and another portion separating from the coast to flow east along the equator (Figure 1) (Schott et al., 2009). The Great Whirl is generally thought to form during the SW Monsoon (Bruce, 1979; Leetmaa et al., 1982; Beal and Donohue, 2013) likely generated by the barotropic instability (Jensen, 1991). The Great Whirl strengthens into August and September (Fischer et al., 1996) before collapsing with the end of the monsoon due to eastward and downward energy transfer, rather than due to relaxation of the wind (Jensen, 1991). The Great Whirl has been observed extending into the subsurface down to 1000

m (Schott and McCreary, 2001). The Southwest Monsoon Current (SMC) flows southeastward along the coast of India during the SW Monsoon.

Much of the surface current direction in the NW Indian Ocean reverses during the NE Monsoon. The Northeast Monsoon Current (NMC) flows westward into the NW Indian Ocean, which contributes to the West India Coastal Current (WICC) flowing northwestward along the coast of India (Bruce et al., 1994). Vinayachandran and Nanjundian (2009) showed in their model that during the NE monsoon, the Northeast Monsoon Current (NMC) transports low-salinity surface water from the Bay of Bengal (NE Indian Ocean) into the NW Indian Ocean. During the SW monsoon, increased evaporation results in the formation of high-salinity surface water in the Arabian Sea (Wajsowicz and Schopf, 2001), which is then transported into the Bay of Bengal by the Southwest Monsoon Current (SMC). The eastward transport is forced by asymmetry in the salinity-induced density difference across the northern Indian Ocean as well as wind forcing (Vinayachandran and Nanjundian, 2009).

The intermonsoonal seasons are represented by high-variability circulation as wind direction changes. Wyrtki (1973) identified high-velocity eastward flowing equatorial jets (Wyrtki Jets) forming during both the boreal spring and fall transitional periods.

The seasonal variations of intermediate depth circulations could also be affected by the seasonal changes of water masses in the study region. The Arabian Sea is a region with strong seasonal and inter-annual changes in salinity and temperature due to the complex water masses interaction and complicated seasonal circulations (Shetye et al. 1991). The geostrophic currents in the subsurface regime due to Ekman suction show a seasonal cycle in the open ocean (Shetye et al., 1991). Investigating the seasonal variations of surface and subsurface

ocean current velocities from observation data as well as temperature and salinity distribution can contribute to understanding the seasonal variations of the intermediate depth circulations.

1.2 Motivation

Until recently, detailed circulation studies have been limited to the upper water column, mainly due to the limitation of data availability (Shi et al., 2000), with more detailed surface studies emerging with the introduction of surface drifters (Molinari et al., 1990), satellite altimetry (Périgaud and Delecluse, 1992), and ship surveys through the World Ocean Circulation Experiment (WOCE). With the WOCE also came the large-scale deployment of subsurface autonomous floats for mapping hydrographic data near 1000 m depth. Davis (2005) used WOCE autonomous float data (primarily ALACE floats) to describe the flow conditions and variability at 900 m depth, calculating mean velocity (2.5° by 2.5° grid) after removing seasonal variability.

The establishment of the Array of Real-time Geostrophic Oceanography (ARGO) program in 2000 provided the ability to collect continuous temperature, salinity and velocity measurements with autonomous floats as deep as 2000 m (Gould et al., 2004; Lebedev et al., 2007). ARGO data have been assessed extensively for reliability (Lebedev et al., 2007) and subsurface analyses have been performed world-wide (Speich et al., 2012; Ollitrault and Rannou, 2013), including a study of characteristics and behavior of regional flow and water masses in the Sea of Oman and northern Arabian Sea after a cyclone passage (Wang et al. 2013).

In this study, an 8-year dataset from ARGO is utilized to provide a high-resolution, quantitative description of intermediate and deep circulation at depths of 1000 m, 1500 m and 2000 m in the northwest Indian Ocean, as well as surface drifter data for surface circulation

analysis. Compared to previous studies in this region, this study has a larger data base and resulting in an increased statistical significance. Velocities obtained from ARGO and surface drifter data were then compared to the Simple Ocean Data Assimilation (SODA) 2.1.6 reanalysis dataset. This study is motivated by the following questions:

- What spatial patterns of horizontal current velocities are identified at the surface and subsurface? In previous studies (particularly in the subsurface), mean circulation has been as assessed over a large geographical region, resulting in a low-resolution grid for the NW Indian Ocean (Davis, 2005; Lebedev et al., 2007). Can a higher resolution analysis improve understanding of mean circulation?
- How do the velocities and current patterns at the surface compare to those in the subsurface? While circulation patterns in the upper 1000 m have been described, the extent to which surface circulation patterns may propagate at depths greater than 1000 m remains elusive.
- How do circulation patterns change seasonally? In previous studies, filtering of seasonal variability has masked seasonal circulation features, such as the Great Whirl (Davis, 2005).
- How does the SODA reanalysis output compare to observational data produced by ARGO floats and surface drifters?

2. Data and Methods

Data were processed and analyzed by boreal seasons, which are roughly aligned with the timing of the NE and SW monsoons, and intermonsoonal periods. Spring is defined as

March-May, summer is defined as June-August, fall is defined as September-November, and winter is defined as December-February.

2.1 ARGO Floats

ARGO data are made freely available by the International ARGO Project and associated contributing national programs (JCOMMOPS ARGO, 2008; UCSD ARGO, 2011). ARGO is a contribution to the Global Ocean Observing System (Feder, 2000; ioc-goos.org). More details about ARGO and its operational principles are available at the ARGO webpage: http://www.argo.ucsd.edu. 175 floats had trajectories within the defined area from January 2002-December 2009. One full float cycle (beginning with descent and ending with resurfacing) lasts 10 days during which the float remains at its cruising depth (i.e. predetermined pressure) for nine days. The trajectory of each float was carefully examined to determine whether latitude and longitude data were unrealistic or were on land. When a coordinate was determined to be unreliable, the entire profile associated with that location was excluded from further analysis. A total of 158 floats were used in this analysis, with cruising depths of 1000 m (101 floats), 1500 m (13 floats), or 2000 m (44 floats). Velocities were calculated using reported time and location at each station (Δ great arc length/Δ time) and separated into north/south and east/west velocity components. At a given depth, velocities greater than 3 standard deviations of all velocities at that depth were excluded. This restriction accounted for less than 1% of the data. To construct velocity fields in the subsurface, the drifting depth of each ARGO float was determined (1000 m, 1500 m and 2000 m). Although there is error associated with raw velocity calculations due to vertical shear stress and surface currents (Lebedev et al., 2007; Ollitraut and Rannou, 2013), Lebedev et al. (2007) and Ollitraut et al. (2006) found when

assessing mean circulation, errors were an order of magnitude smaller than the velocity values (only on the order of mm/s). For this reason, the error was assumed to be negligible in this study.

Because significant spatial and temporal variability existed in the individual velocity observations within a geographic region, velocity data were averaged to generate maps for each season at 1000 m, 1500 m and 2000 m, following the Lagrangian averaging scheme of DiMarco et al. (2005). Velocity data in each 2° by 2° box were averaged when at least three velocity vectors were present. For boxes with less than three velocity vectors, mean velocity was not plotted. The box was then shifted by 1°, i.e. 50% overlap of 2˚x2˚ boxes, and the same process was performed. Using this technique, it was considered that every other velocity vector could be regarded as independent. Variance ellipses were also calculated for each 2˚x2˚ box and plotted with mean velocity vectors on the same map.

2.2 Surface Drifters

Monthly and annual mean surface velocity data from the Global Drifter Array were obtained from the Drifter-Derived Climatology of the Atlantic Oceanographic and Meteorological Laboratory (Lumpkin and Garraffo, 2005; Lumpkin and Pazos, 2006; NOAA/AOML). Climatology includes data from March 1995 through March 2009. Each drifter consists of a surface buoy and a subsurface drogue. The drogue is centered at 15 m depth. The buoy has a transmitter, which sends measurements and GPS coordinates to satellites. The resulting velocity of the drifter is a combination of currents at 15 m depth, plus upper-ocean wind-driven flow, and drifter “slip” (Lumpkin and Pazos, 2006). Surface velocity maps were produced from surface drifter data using the same technique used for ARGO velocity averaging.

2.3 SODA Climate Reanalysis

Multiple data sources are used in constructing the SODA climate reanalysis dataset, which ingests a wide variety of observations including hydrographic profiles, ocean station data, moored temperature and salinity measurements, surface temperature and salinity observations from a variety of instruments, sea surface temperature and sea level altimetry from satellites. The circulation assimilation is based on Los Alamos National Laboratory Parallel Ocean Program (POP) (Carton et al., 2000; Carton and Giese, 2008). SODA 2.1.6 output has a horizontal resolution of 0.25° x 0.4° and 40 vertical levels with 10-m spacing near the surface. The SODA dataset was chosen for its resolution and because it does not assimilate ARGO or surface drifter velocity observations at any time. Because SODA is widely used to provide initial boundary conditions for other regional numerical models, it is valuable to examine how the SODA reanalysis circulations compared to those derived from the two independent observations based on ARGO and surface drifters.

Horizontal velocity fields from SODA were generated at 1000 m, 1500 m, and 2000 m depth for each season from 1992-2001. Initial velocity plots had a spatial resolution of 0.5 degrees occurring at 0.25 and 0.75 within each degree. Seasonal velocity plots produced from SODA were averaged in the same way as the ARGO seasonal velocity plots, i.e., by averaging all velocities within a 2˚x2˚box, and shifting the box 1˚ at a time. Vector correlations (Crosby et al., 1993), scalar correlations and the statistical significance of the scalar correlations were calculated for locations in which both observations and SODA output exist.

3. Results and Discussion

3.1 SW Summer Monsoon

Surface and subsurface current velocities during the SW Monsoon are shown in Figure 2. Flow direction in the Arabian Sea is primarily to the east and southeast down to 2000 m, which is consistent with ship drift observations. Observations of current velocity are more sparse at 2000 m, but indicate a similar eastward/southeastward flow. Average velocity in the Arabian Sea is around 30 cm/s at the surface, and decreases to 5 cm/s at 1000 m, and 3 cm/s at 2000 m.

The Somali Current is observed flowing northeastward along the Somali coast at the surface, with largest mean velocities up to 179.5 cm/s occurring in the summer (Figure 2a). Northeastward coastal flow is also observed at 1000 m (Figure 2b) and 1500 m (Figure 2c), with summer mean velocities up to 26.1 cm/s at 1000 m, which are comparable to EACC velocities of 20 cm/s at 1000 m observed by DiMarco et al. (2002). The Somali Current is accompanied by the formation of several offshore anticyclonic eddies. The largest of these eddies is the Great Whirl, which forms near the Horn of Somalia (Bruce, 1979; Jensen, 1991; Schott et al., 2009; Beal and Donahue, 2013), and exhibits maximum surface velocities of 161.4 cm/s. This velocity obtained from surface drifters is greater than observations (120 cm/s in June, decreasing to 70 cm/s by September) by Beal and Donahue (2013) during the summer of 1995. This suggests that some SW Monsoon seasons may result in enormously high surface velocities that increase the average velocities observed in this study. Mooring measurements (Schott and McCreary, 2001) from July to September 1995 indicate the Great Whirl reaches an average depth of 1000 m during the SW Monsoon, with speeds of 10 cm/s. This is consistent with ARGO velocity measurements observed at 1000 m averaged from June to August (Figure 2b), with maximum velocities of 16.2 cm/s. Observations from surface drifters show an average diameter of 400-

500 km, which is consistent with Beal and Donahue (2013) who measured diameters of 350 km and 540 km in June and September, respectively.

The East Arabian Current (EAC) flows northeastward along the southern coast of Oman during the summer (Figure 2a) and early fall (Figure 5). Velocity decreases as the Somali Current transforms to the EAC, with maximum EAC surface velocities of 52.3 cm/s in the west (Figure 2a). The EAC extends beyond Cape Ras al Hadd to the east/northeast (becoming the Ras al Hadd Jet once off the cape), with observed velocities ranging from 20-40 cm/s. In Böhm et al. (1999), Ras al Hadd Jet velocities were quantified as ranging from 50-70 cm/s, with some velocities as high as 100 cm/s. The velocities seen from surface drifter data are likely muted due to low spatial resolution and spatial averaging of the data.

A uniform eastward flow along the equator is observed at the surface, 1000 m and 1500 m, which includes the portion of the EACC that separates from the coast upon crossing the equator. The Southwest Monsoon Current (SMC) is observed flowing southeastward along the west coast of India, with mean surface velocities up to 51.2 cm/s (Figure 2a). A southeastward flow is also observed at 1000 m (Figure 2b) and 2000 m (Figure 2d) along the coast of India, with velocities up to 8 cm/s; however, since the SMC is restricted to the near-surface (Schott et al., 1994), the subsurface flow patterns observed from ARGO here are likely not associated with the surface SMC.

3.2 NE Winter Monsoon

Much of the flow direction reverses from the summer to the winter (Figure 3). Maximum mean surface velocities occur in the Somali Current, flowing southwestward along

the coast of Somalia up to 97.3 cm/s. Southwestward flow along the Somali coast is also observed at 1000 m and 1500 m (up to 10 cm/s).

The Northeast Monsoon Current (NMC) extends to the North Equatorial Current (NEC), which is observed flowing westward at 5°N at the surface (Figure 3a). This is a flow reversal from that seen in the summer. Mean surface velocity of the NEC is 28.5 cm/s. The westward current diverges at the Somali coast at the surface (Figure 3a), 1000 m (Figure 3b), and 1500 m (Figure 3c), with a small portion flowing northward and a majority flowing southward with the Somali Current, demonstrating the complicated Somali current system and its associated eddies (Jensen, 1991).

In the Gulf of Aden, patterns indicate a westward surface current with mean velocities ranging from 8.3-40.2 cm/s (Figure 3a). Westward flow is also present at 1000 m in the Gulf of Aden (8 cm/s). In the Sea of Oman, calculated velocities indicate an eastward flow at 1000 m ranging from 2-5 cm/s. Large variance of 6-12 $(cm/s)^2$ is associated with the mean velocities in the Gulf of Aden and Sea of Oman at 1000 m (Figure 3b). The WICC (Figure 1) is not observed in surface drifter data (Figure 3a).

3.3 Spring Intermonsoon

The spring is an intermonsoonal period, with high variability in current speed and direction (Figure 4) as the wind transitions between from the NE to the SW monsoon. The Somali Current flows to the northeastward at the surface with a maximum mean surface velocity of 67.7 cm/s. The Great Whirl is already observed near the Somali coast at the surface and 1000 m, exhibiting surface velocities near 30 cm/s. Schott and McCreary (2001) observed that the Great Whirl usually forms in June and lasts through the SW Monsoon. However, both

ARGO (1000m) and surface drifter data suggest that it could form earlier during the spring inter-monsoon, which is in contrast to previous studies. More investigations are needed to understand the timing and formation of the Great Whirl. Surface flow is westward between 3°N-6°N from 40°E-60°E, with velocities up to 25.1 cm/s. North of this region (8°N and 10°N), flow is eastward. Surface velocities in the Gulf of Aden are uniformly to the west (up to 29.3 cm/s). Large variance occurs along the coastlines at 1000 m and 1500 m and is likely due to reversing flow direction associated with the seasonal transition. Notably, the Wyrtki Jets are not distinct from surface drifter data. There is a generally eastward flow along the equator from 65° to 80°, with velocities ranging from 10 to 40 cm/s, which are considerably less than the 60-215 cm/s velocities noted in Wyrtki (1973). It is possible that velocities could be muted due to spatial and seasonal averaging, or that the greatest velocities occur south of the equator, which is outside the bounds of this study.

3.4 Fall Intermonsoon

Fall intermonsoonal circulation is variable as wind patterns transition from the SW to the NE Monsoon (Figure 5), though less variable than spring intermonsoonal circulation. The Somali Current flows northeastward along the Somali coast at the surface, with maximum mean surface velocities of 140 cm/s (Figure 5). Flow separates from the coast at several locations forming anticyclonic circulation. The East Arabian Current continues along the coast of Oman, continuing to the east and northeast off Cape Ras al Hadd. Surface velocities off Cape Ras al Hadd are smaller (20-50 cm/s) during the fall (Figure 5a) than those observed in the summer (Figure 2a).

The Great Whirl can still be observed during the fall intermonsoon at the surface, 1000 m, and 1500 m, with weaker velocities than those observed during the SW monsoon. Flow is to the west in the Gulf of Aden at the surfrace and 1000 m. Unlike the spring intermonsoon, strong eastward equatorial flow associated with the Wyrtki Jets is observed along the equator, with surface velocities ranging from 40 to 70 cm/s east of 60°E. Eastward flow is also observed at 1000 m (14.8 cm/s) and 2000 m (7.2 cm/s). Similarly to spring intermonsoon, fall intermonsoonal velocities along the coast and those associated with eddy or gyre circulation have large variance. Coastal velocity variance typically ranges from 5-18 $(cm/s)^2$, with velocity variance exceeding 20 $(cm/s)^2$ at 1000 m at points along the Somali coast (Figure 5b).

3.5 SODA Output Comparison

Figures 6-9 show mean velocities at the surface, 1000 m, 1500 m, and 2000 m produced from SODA reanalysis output. Several similarities can be seen in the observed current patterns (Figures 2-5) and the SODA reanalysis output (Figures 6-9), with the best qualitative agreement occurring in the summer (Figures 2 and 6). The highest surface velocities in the SODA output are observed along the Somali coast flowing to the northeast (134.3 cm/s); however, the distinct northeastward flow observed along the Somali coast in the subsurface (Figure 2) is not produced in SODA output (Figure 6). While the data show the Great Whirl extending from the surface to 1000 m, SODA output displays the Great Whirl only at the surface with velocities (10.1-107.6 cm/s). The East Arabian Current is present in SODA output with velocities up to 39.5 cm/s. Eastward flow is produced at 1000 m (Figure 6b) and 1500 m (Figure 6c) in SODA output with velocities around 4 cm/s.

Winter surface currents observed from surface drifter data (Figure 3a) can also be seen in SODA output (Figure 7), including the Somali Current (55 cm/s), North Equatorial Current (46 cm/s), and Northeast Monsoon Current (54 cm/s). The WICC which was not observed in the surface drifter data (Figure 3a), is produced in the surface SODA output with surface velocities up to 32.3 cm/s and a current width of approximately 300 km (Figure 7a). The width of the WICC produced here is comparable to observations made in Shetye et al. (1991). Westward flow in the Gulf of Aden and cyclonic circulation to the east of the Gulf of Aden are also observed in the surface SODA output. In the data at the surface, 1000 m, and 1500 m, westward flow between 5°N-10°N diverges as it approaches the Somali coast. This divergence is produced in the SODA output at all depths. In the subsurface at 1000 m and 1500 m, the assimilation shows this flow as part of a large anticyclonic circulation cell from 50°E-70°E and 5°N-12°N. The portion that flows northward separates from the coast at 10°N and flows eastward/northeastward through 70°E. At this location, flow redirects to the southwest and continues as westward flow toward the Somali coast.

In the spring at the surface, the SODA output (Figure 8a) and drifter data (Figure 4a) both show a westward flow along 5°N. In the SODA output, the surface flow diverges at the Somali coast. The northward flow diverges as it passes the Horn of Somalia, either flowing westward through the Gulf of Aden, or continuing northeastward along the Oman coast. At 1000 m and 1500 m, westward flow occurs between 5°N and 10°N, which diverges at the Somali coast. The southward-flowing portion is part of a recirculation cell, which can be seen at all subsurface depths from 3°N-7°N and 50°E-60°E.

In the fall at the surface (Figure 9a), a northeastward flowing Somali Current (30-70 cm/s) and Great Whirl are present in the assimilation. The Great Whirl is not produced in the subsurface in the SODA output. Surface velocities off Cape Ras al Hadd are much smaller in the SODA output (11.9 cm/s) compared to average velocities observed in surface drifter data (20-50 cm/s). At all subsurface depths, flow along the Somali coast is to the southwest with velocities up to 5 cm/s.

Point-by-point vector and scalar correlations of SODA output to ARGO and surface drifter data were calculated and are shown in Table 1. Surface SODA output and surface drifter data generally produced a strong vector correlation, ranging from 0.71-0.93, while subsurface scalar correlations and 92% of vector correlations were < 0.40. All surface scalar correlations produced p-values of 0.00. Stronger correlations during the summer and winter surface velocities can be attributed to surface currents strongly controlled by the SW and NE monsoons. Weaker correlations for spring and fall are likely due to variability associated with intermonsoonal transitions.

Directional patterns observed in the surface velocities generally agreed between the observation and SODA reanalysis output; however, SODA output generally underestimates velocities compared to the observations. Histograms of SODA output minus observations from surface drifters and ARGO floats are shown in Figure 10 for each season and depth. The histograms (Figure 10) and the correlations (Table 1) for subsurface velocities demonstrate that while current patterns generally agree, there is disagreement in scalar values, likely due to limitations in the SODA reanalysis, e.g. smoothing of bathymetry, bottom roughness, and wind

fields. Furthermore, the SODA reanalysis does not assimilate the addition of high-salinity water masses from the Red Sea and Persian Gulf (Carton et al., 2000; Carton and Giese, 2008), which will impact resulting subsurface velocity output, particularly along the coast. Assimilating adequate representation of interactions between the Red Sea and Persian Gulf as well as assimilating ARGO velocities into the SODA reanalysis could result in improved subsurface velocity fields, especially during the fall and spring when observations suggest that flow is highly variable.

4. Conclusion

This circulation investigation of the Northwest Indian Ocean provides a 1°x1°-resolution quantitative analysis of surface and subsurface velocities, and investigates large scale intermediate (at 1500 m and 2000 m) circulation patterns for the first time. Although large-scale circulation in this region has been assessed in the past, low resolution analyses have masked smaller features, and data were not analyzed by season. The complexity of the region, and its dependence on seasonal atmospheric wind conditions warranted a high-resolution, seasonal assessment.

The presence of major surface currents could be identified in the surface drifter data (except for the West India Coastal Current in surface drifter data). During the SW Monsoon, surface currents (and maximum averaged velocities from surface drifter data) include the Somali Current (179.5 cm/s), East Arabian Current (52.3 cm/s), Southwest Monsoon Current (51.2 cm/s), and the Great Whirl (161.4 cm/s). In contrast to previous studies, both ARGO and surface drifter data show the Great Whirl can form as early as the Spring intermonsoon, lasting

until the Fall intermonsoon. During the NE Monsoon, identified surface currents include the Somali Current (97.3 cm/s), North Equatorial Current (28.5 cm/s), and Northeast Monsoon Current (30.0 cm/s). A SODA reanalysis comparison to surface drifter data produced vector correlations of 0.71-0.93, and scalar correlations of 0.40-0.72.

ARGO float and surface drifter data can provide detailed information about circulation patterns and current velocities when averaged over long time periods. Although short-term event circulation could be analyzed, the spatial coverage of ARGO and surface drifters may limit data availability and reliability for a particular region; thus, data averaged over longer time periods provides more spatial coverage for a region. Continued measurements, especially subsurface ARGO float measurements, will provide more data for assessing seasonal circulation patterns at 1500 m and 2000 m.

Acknowledgements

We would like to thank Lighthouse R & D Enterprises, Inc. and Texas A&M University for providing financial support for this project. Additional funding was received through NSF-STEM and Scherck Fellowships. We thank B. Giese (TAMU) for access to the SODA model output. Thanks to Piers Chapman and Ken Bowman (TAMU) for their valuable comments during the early development of this manuscript. Finally, we would like to thank the data providers, Rick Lumpkin with the NOAA Global Drifter Program, and UCSD/JCOMMOPS. ARGO data were collected and made freely available by the International ARGO Project and the national programs that contribute to it.

References

Beal, L.M. and Donohue, K.A., 2013. The Great Whirl: Observations of its seasonal development and interannual variability. J Geophys Res, 118:1-13.

Böhm, E., Morrison, J.M., Manghnani, V., Kim, H., and Flagg, C.N., 1999. The Ras al Hadd Jet: and acoustic Doppler profiler observations in 1994-1995. Deep-Sea Res Pt II, 46:1531-1549.

Bruce, J.G., 1979. Eddies off the Somali Coast During the Southwest Monsoon. J Geophys Res, 84:7742-7748.

Bruce, J.G., Johnson, D.R., and Kindle, J.C., 1994. Evidence for eddy formation in the eastern Arabian Sea during the northeast monsoon. J Geophys Res, 99:7651-7664.

Carton, J. A., Chepurin, G., Cao, X., and Giese, B., 2000. A simple ocean data assimilation analysis of the global upper ocean 1950-95. Part I: Methodology. J Phys Oceanogr, 30:294-309.

Carton, J. A. and Giese, B.S., 2008. A reanalysis of ocean climate using simple ocean data assimilation (SODA). Mon Weather Rev, 136:2999-3017.

Crosby, D. S., Breaker, L.C., and Gemmill, W. H., 1993. A proposed definition for vector correlation in geophysics: theory and application. J Atmos Ocean Tech, 10:355-367.

Davis, R.E., 2005. Intermediate-Depth Circulation of the Indian and South Pacific Oceans Measured by Autonomous Floats. J Phys Oceanogr, 683-707.

DiMarco, S. F., Chapman, P., Nowlin, W. D., Hacker, P., Donohue, K., Luther, M., Johnson, G., and Toole, J., 2002. Volume transport and property distributions of the Mozambique

Channel. Deep-Sea Res Pt II, 49:1481-1511.

DiMarco, S. F., Nowlin, Jr., W. D., and Reid, R. O., 2005. A Statistical Description of the Near-surface Velocity Field from Drifters in the Gulf of Mexico: Geophysical Monograph Series. Circulation in the Gulf of Mexico: Observations and Models. Eds. W. Sturges and A. Lugo-Fernandez. American Geophysical Union, 161:101-110.

Feder, T., 2000. Argo begins systematic global probing of the upper oceans. Phys Today, 53:50–51.

Fischer, J., Schott, F., and Stramma, L., 1996. Currents and transports of the Great Whirl-Socotra Gyre system during the summer monsoon, August 1993. J Geophys Res, 101:3573-3587.

Gould, W.J., Roemmich, D., Wuffels, S., Freeland, H., Ignaszewsky, M., Jianpink, X., Pouliquen, S., Desaubies, Y., Send, U., Radhakrishnan, K., Takeuchi, K., Kim, K., Danchenkov, M., Sutton, P., King, B., Owens, B., and Riser, S., 2004. Argo Profiling Floats Bring New Era of In Situ Ocean Observations. Eos, 85:179, 190-191

Izumo, T., Montégut, C.B., Luo, J.J., and Behera, S.K., 2008. The role of the western Arabian Sea upwelling in Indian monsoon rainfall variability. J Clim, 21:5603-5623.

JCOMMOPS ARGO, unpublished data, 2008. Available from Joint WMO-IOC Technical Commission for Oceanography and Marine Meteorology in situ Observing Platform Support Centre (http://ARGO.jcommops.org).

Jensen, T. G., 1991. Modeling the seasonal undercurrents in the Somali Current system. J Geophys Res, 96:22151-22167.

Lebedev, K.V., Yoshinari, H., Maximenko, N.A., and Hacker, P.W., 2007. YoMaHa'07: Velocity data assessed from trajectories of Argo floats at parking level and at the sea surface.

IPRC Technical Note, 4(2).

Leetmaa, A. and Quadfasel, D.R., 1982. Development of the flow field during the onset of the Somali Current, 1979. J Phys Oceanogr, 12:1325-1342.

Lumpkin, R. and Garraffo, Z., 2005. Evaluating the decomposition of Tropical Atlantic drifter observations. J Atmos Ocean Tech, 22:1403-1415.

Lumpkin, R. and Pazos, M., 2006. Measuring surface currents with surface velocity program drifters: the instrument, its data, and some recent results. Eds: Griffa, A., Kirwan, A.D., Mariano, A.J., Ozgokmen, T., and Rossby, T., Lagrangian Analysis and Prediction of Coastal and Ocean Dynamics (LAPCOD). Cambridge University Press, Cambridge, New York, 39-67.

McCreary, J. P. and Kundu, P. K., 1989. A numerical investigation of sea surface temperature variability in the Arabian Sea. J Geophys Res, 94:16097-16114.

McCreary, J. P., Yu, Z., Hood, R. R., Vinaychandran, P. N., Furue, R., Ishida, A., & Richards, K. J., 2013. Dynamics of the Indian-Ocean oxygen minimum zones. Prog Oceanogr, 112:15-37.

Molinari, R.L., Olson, D., and Reverdin, G., 1990. Surface current distributions in the tropical Indian Ocean derived from compilations of surface buoy trajectories. J Geophys Res, 95:7217-7238.

Morrison, J. M., L. A. Codispoti, S.L. Smith, K. Wishner, C. Flagg, W.D. Gardner, S. Gaurin, S.W.A. Naqvi, V. Manghani, L. Prosperie, and J.S. Gundersen, 1999. The oxygen minimum zone in the Arabian Sea during 1995. Deep-Sea Res II, 46(8/9):1903–1931.

Ollitrault, M., Lankhorst, M., Fratantoni, D., Richardson, P., and Zenk, W., 2006. Zonal intermediate currents in the equatorial Atlantic Ocean. Geophys Res Lett, 33:1-4.

Ollitrault, M. and Rannou, J.P., 2013. ANDRO: An Argo-Based Deep Displacement Dataset. J Atmos Ocean Technol, 30:759-788.

Périgaud, C. and Delecluse, P., 1992. Annual sea level variations in the southern tropical Indian Ocean from Geosat and shallow-water simulations. J Geophys Res, 97:20169-20178.

Piontkovski, S. A. and H. S. Al-Oufi, 2015. The Omani shelf hypoxia and the warming Arabian Sea. Int J Environ Stud, 72(2):256-264.

Schott, F., Reppin, J., Fischer, J., and Quadfasel, D., 1994. Currents and transports of the Monsoon Current south of Sri Lanka. J Geophys Res, 99:25127-25141.

Schott, F. A. and McCreary, J. P., 2001. The monsoon circulation of the Indian Ocean. Prog Oceanogr, 51:1-123.

Schott, F. A., Xie, S., and McCreary, J. P., 2009. Indian Ocean circulation and climate variability. Rev Geophys, 47:1-46.

Shetye, S.R., Gouveia, A.D., Shenoi, S.S., Michael, G.S., Sundar, D., Almeida, A.M., and Santanam, K., 1991. The coastal current off western India during the northeast monsoon. Deep Sea Res Pt I, 38:1517-1529.

Shi, W., Morrison, J. M., Böhm, E., and Manghnani, V., 2000. The Oman upwelling zone during 1993, 1994, 1995. Deep-Sea Res Pt II, 42:1227-1247.

Smith, S. L., and M. Madhupratap, 2005. Mesozooplankton of the Arabian Sea: Patterns influenced by seasons, upwelling, and oxygen concentrations. Prog Oceanogr, 65:214–239

Speich, S., Arhan, M., Rusciano, E., Faure, V., Ollitrault, M., Gent, A.P., and Swart, S., 2012. Use

of Argo Floats to Study the Ocean Dynamics South of Africa: What we have Learned from the Goodhope Project and what we Plan within the Samoc International Programme. Mercator Ocean- Coriolis Quarterly Newsletter, 45, 21.

Tomczak, M., and Godfrey, J. S., 2013. Regional oceanography: an introduction. Butterworth-Heinemann, United Kingdom.

UCSD ARGO, unpublished data, 2011. Available from the University of California at San Diego (http://www.ARGO.ucsd.edu).

Vinayachandran, P. N. and Nanjundiah, R. S., 2009. Indian Ocean sea surface salinity variations in a coupled model. Clim Dynam, 33:245-263.

Wajsowicz, R. C. and Schopf, P. S., 2001. Oceanic influences on the seasonal cycle in evaporation over the Indian Ocean. J Climate, 14:1199-1226.

Wang, Z., DiMarco, S.F., Jochens, A.E., and Ingle, S., 2013. High salinity events in the northern Arabia Sea and Sea of Oman. Deep Sea Res Pt I, 74:14-24.

Wang, Z., S. F. DiMarco, S. Ingle, L. Belabbassi, and L. H. Al-Kharusi, 2014. Seasonal and annual variability of vertically migrating scattering layers in the northern Arabian Sea. Deep Sea Research Part I: Oceanographic Research Papers, 90:152-165.

Wyrtki, K., 1973. An equatorial jet in the Indian Ocean. Science, 181-262-264

Figure Descriptions

Figure 1. NW Indian Ocean Schematic: Known surface currents in the NW Indian Ocean during the (a) SW monsoon and (b) NE monsoon. The currents shown are the Southwest Monsoon Current (SMC), the Northeast Monsoon Current (NMC), the Somali Current (SC), the Great Whirl (GW), the East Arabian Current (EAC), the North Equatorial Current (NEC), and the West India Coastal Current (WICC). Meridional Ekman transport (Me) is indicated by the dashed arrows. Depth contours are in light gray, and indicate the 1000 m and 2000m isobaths. Modified from Schott et al. (2009) and Tomczak and Godfrey (2013).

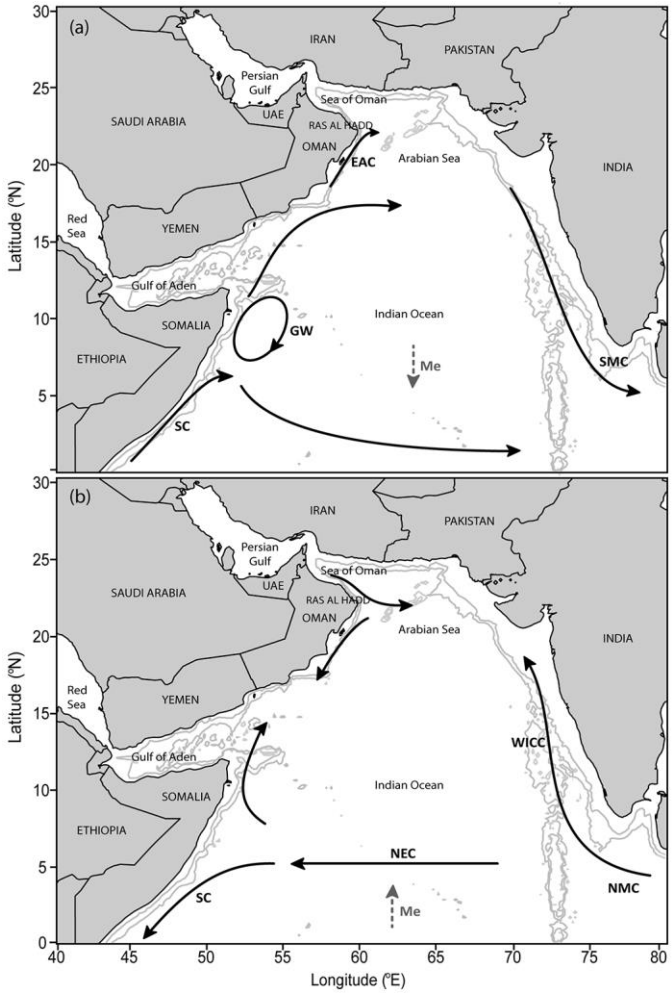

Figure 2. Surface Drifter and ARGO Summer Velocity: Mean summer velocity at (a) the surface, (b) 1000 m with 1000 m isobath and variance ellipses, (c) 1500 m with 1500 m isobath and variance ellipses, and (d) 2000 m with 2000 m isobath and variance ellipses.

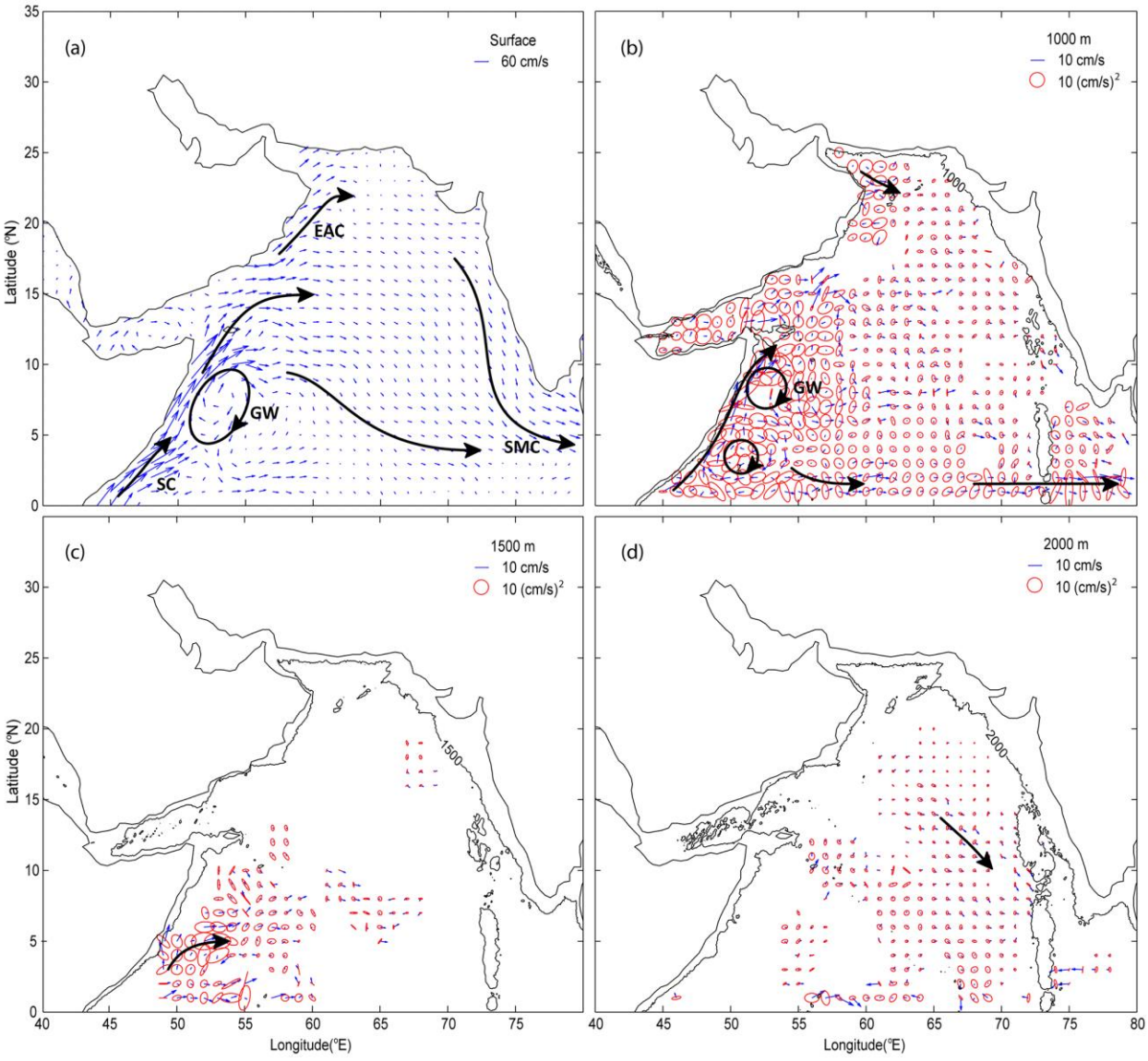

Figure 3. Surface Drifter and ARGO Winter Velocity: Mean winter velocity at (a) the surface, (b) 1000 m with 1000 m isobath and variance ellipses, (c) 1500 m with 1500 m isobath and variance ellipses, and (d) 2000 m with 2000 m isobath and variance ellipses.

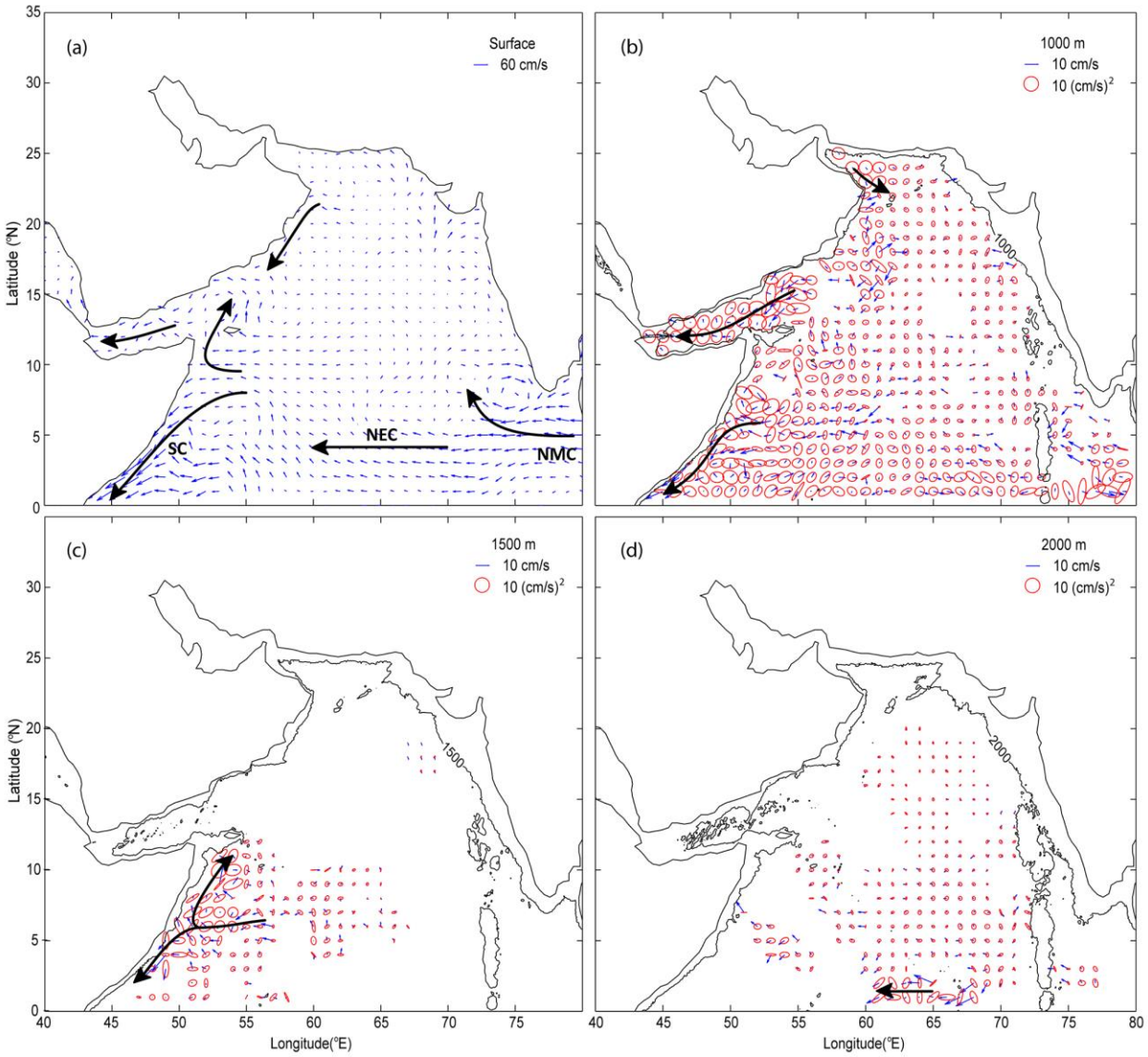

Figure 4. Surface Drifter and ARGO Spring Velocity: Mean spring velocity at (a) the surface, (b) 1000 m with 1000 m isobath and variance ellipses, (c) 1500 m with 1500 m isobath and variance ellipses, and (d) 2000 m with 2000 m isobath and variance ellipses.

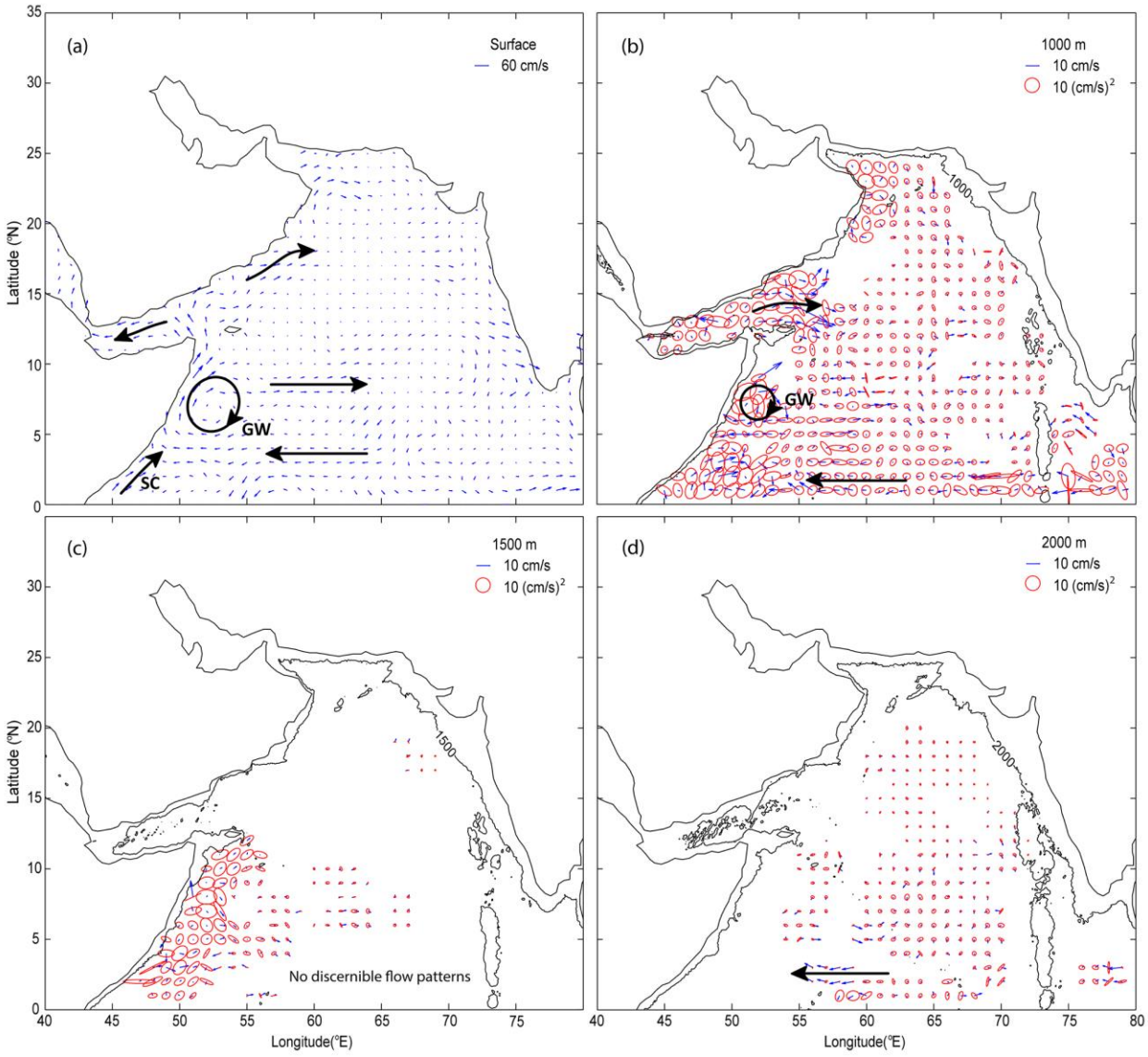

Figure 5. Surface Drifter and ARGO Fall Velocity: Mean fall velocity at (a) the surface, (b) 1000 m with 1000 m isobath and variance ellipses, (c) 1500 m with 1500 m isobath and variance ellipses, and (d) 2000 m with 2000 m isobath and variance ellipses.

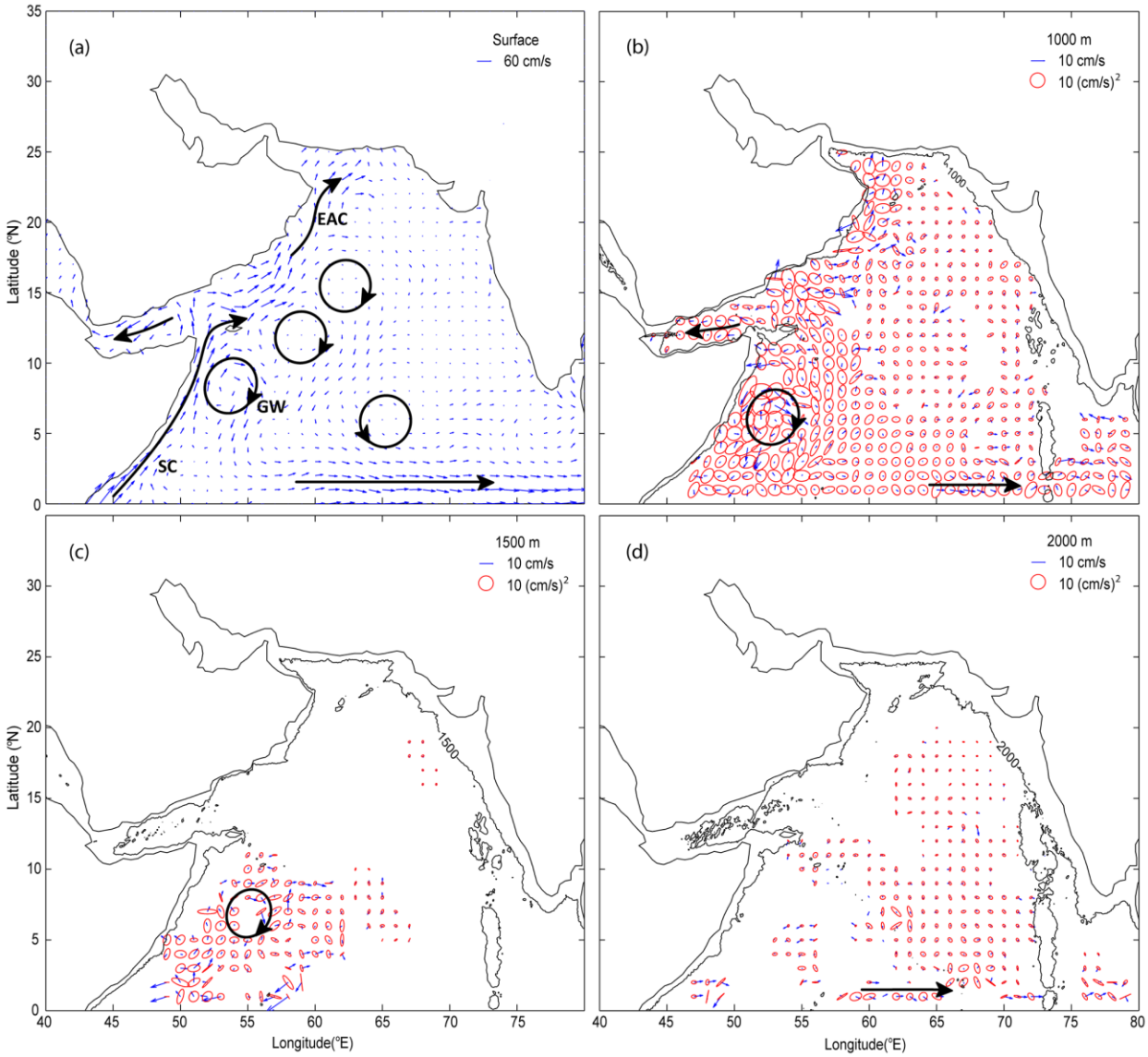

Figure 6. SODA Summer Velocity: Mean summer velocity output from the SODA 2.1.6 1992-2001 reanalysis at (a) the surface, (b) 1000 m with 1000 m isobath and variance ellipses, (c) 1500 m with 1500 m isobath and variance ellipses, and (d) 2000 m with 2000 m isobath and variance ellipses.

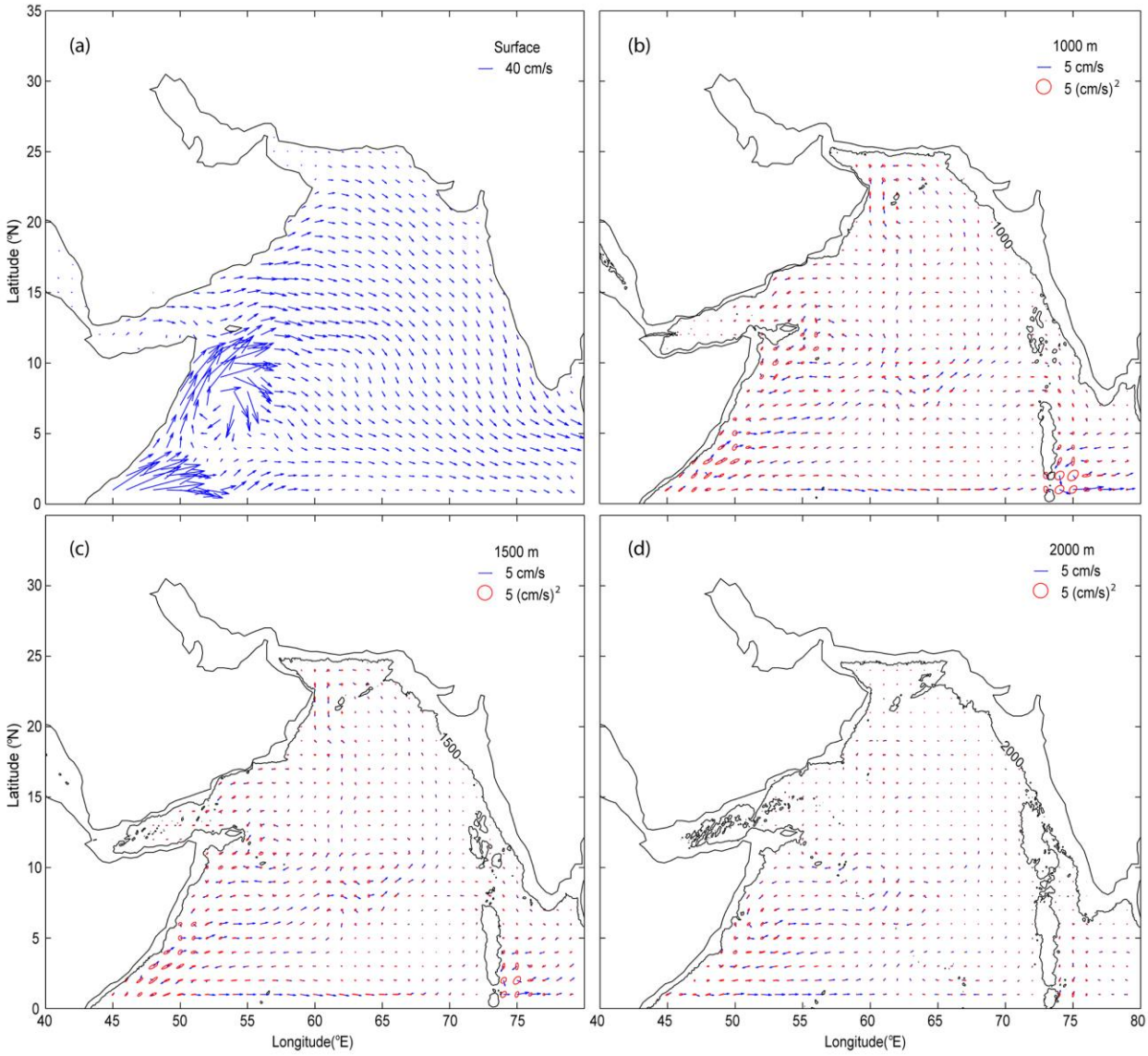

Figure 7. SODA Winter Velocity: Mean winter velocity output from the SODA 2.1.6 1992-2001 reanalysis at (a) the surface, (b) 1000 m with 1000 m isobath and variance ellipses, (c) 1500 m with 1500 m isobath and variance ellipses, and (d) 2000 m with 2000 m isobath and variance ellipses.

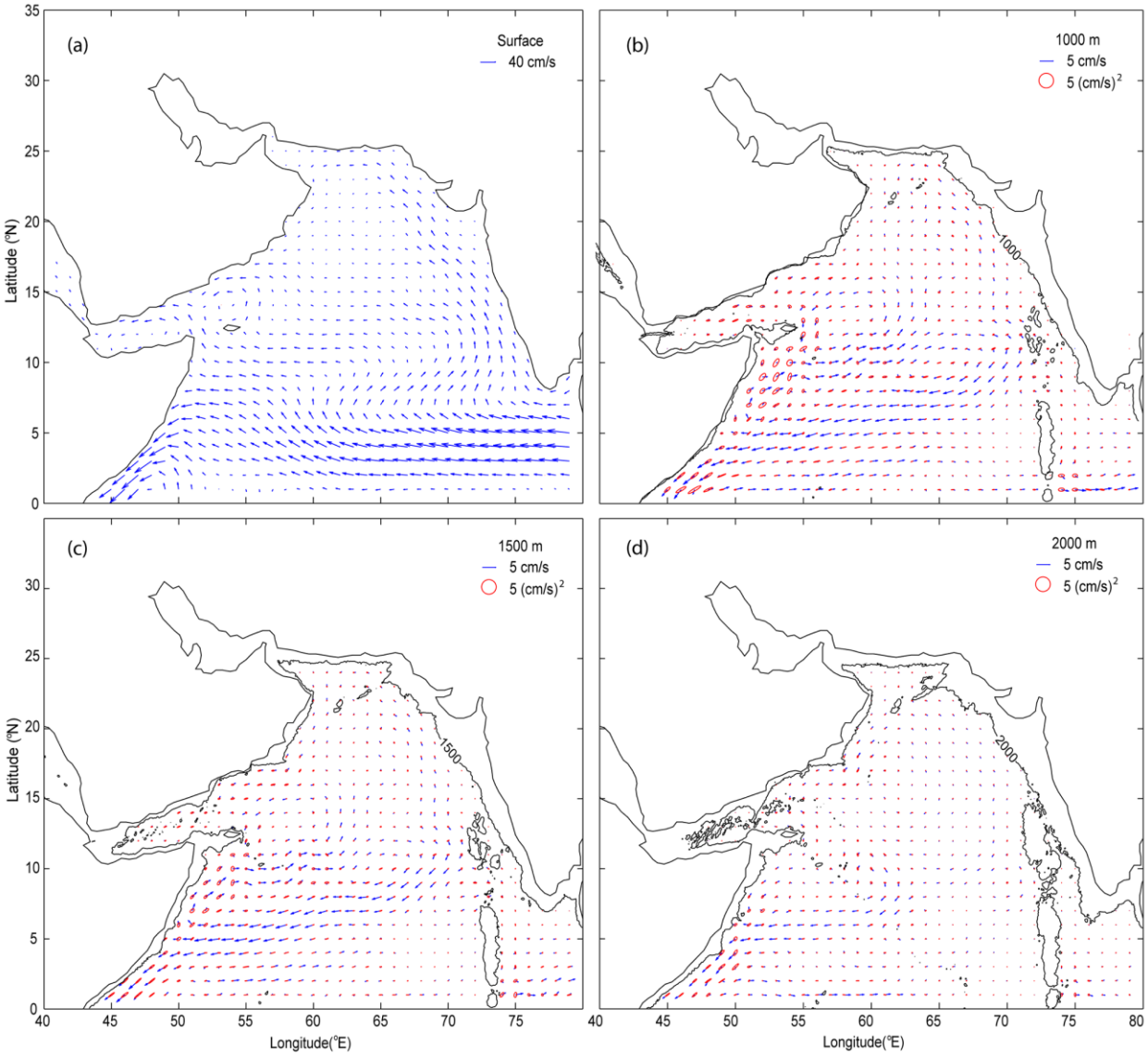

Figure 8. SODA Spring Velocity: Mean spring velocity output from the SODA 2.1.6 1992-2001 reanalysis at (a) the surface, (b) 1000 m with 1000 m isobath and variance ellipses, (c) 1500 m with 1500 m isobath and variance ellipses, and (d) 2000 m with 2000 m isobath and variance ellipses.

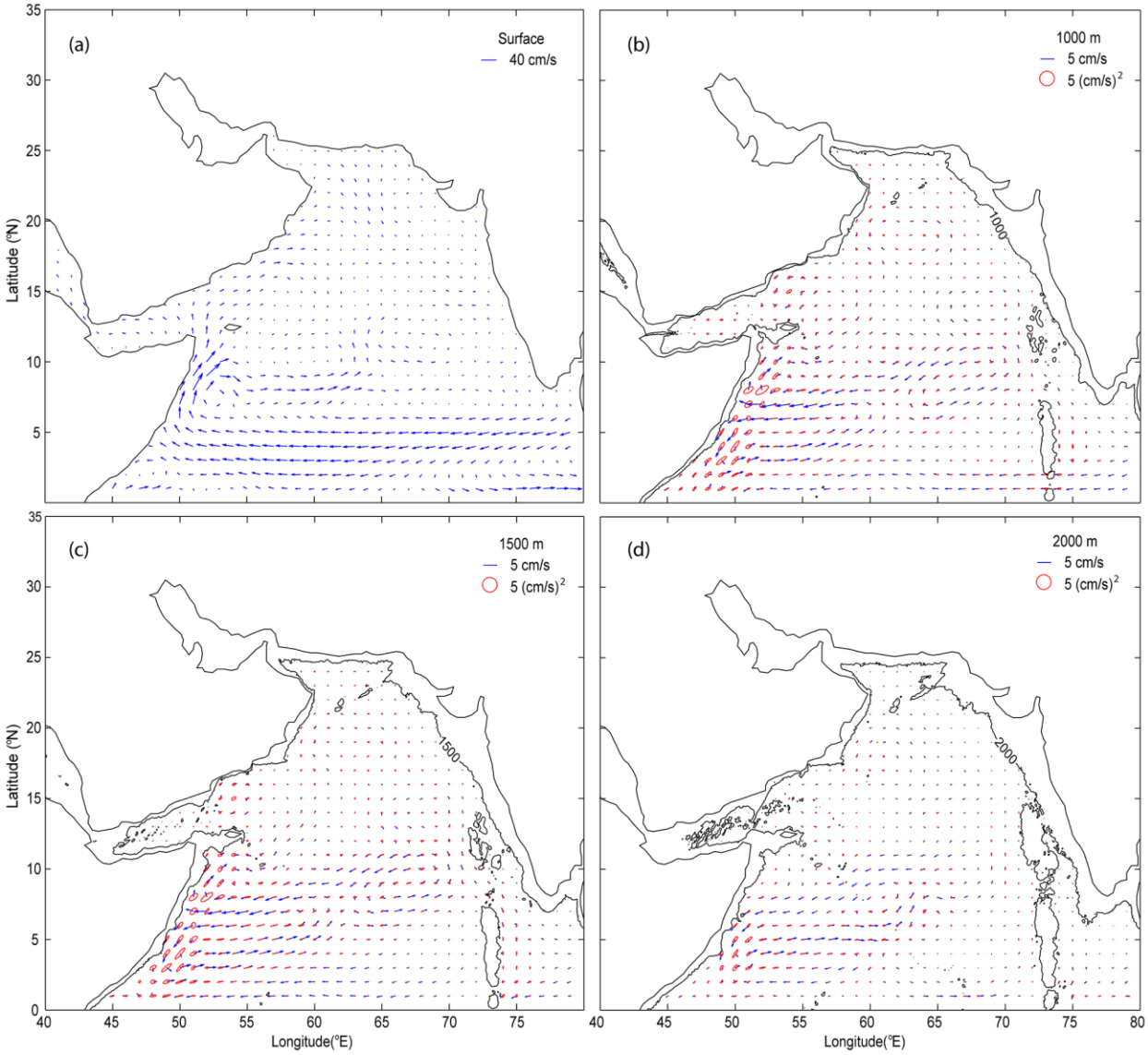

Figure 9. SODA Fall Velocity: Mean fall velocity output from the SODA 2.1.6 1992-2001 reanalysis at (a) the surface, (b) 1000 m with 1000 m isobath and variance ellipses, (c) 1500 m with 1500 m isobath and variance ellipses, and (d) 2000 m with 2000 m isobath and variance ellipses.

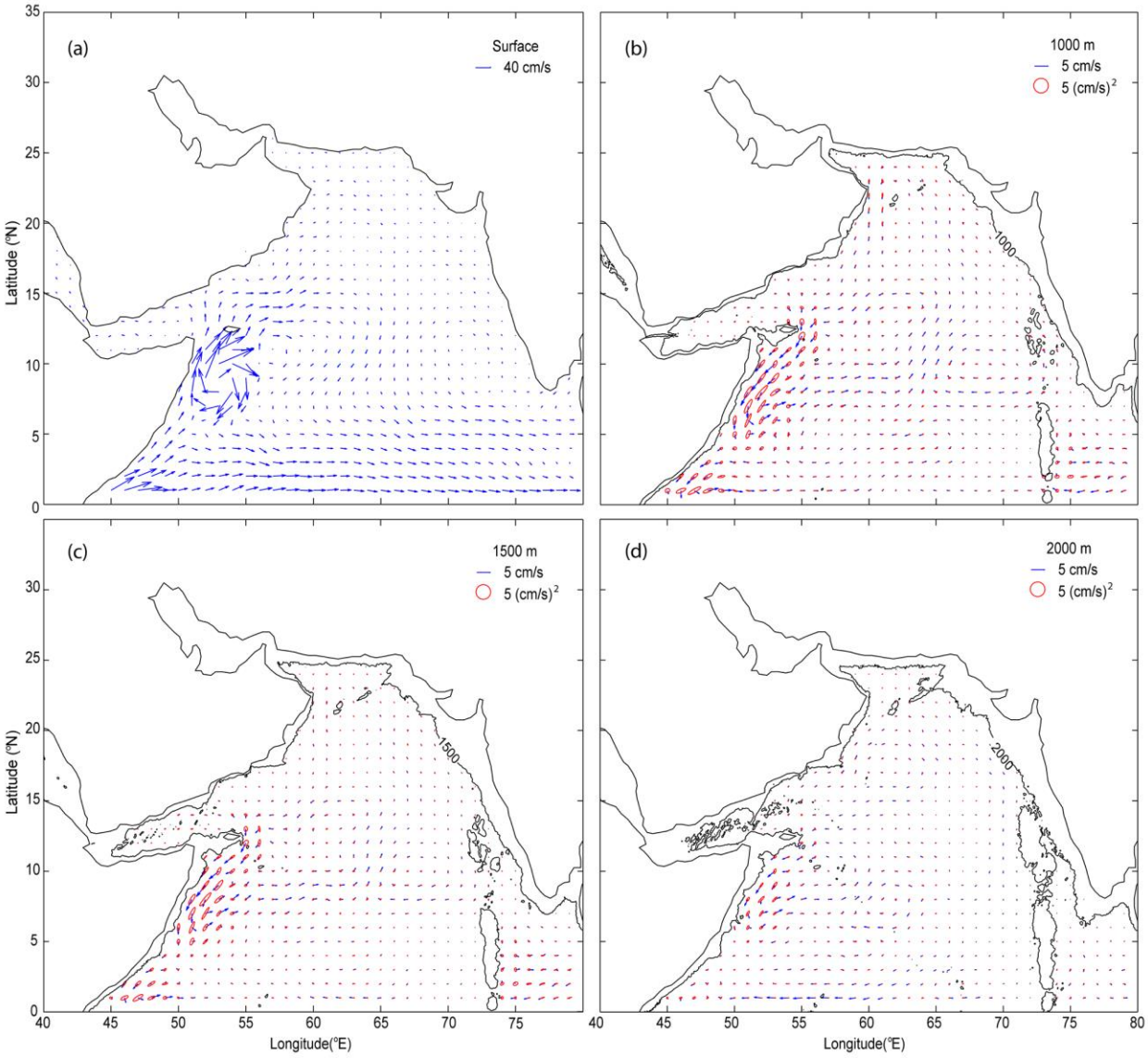

Figure 10. Histograms of scalar SODA reanalysis output minus observations from surface drifters and ARGO floats. All y-axis units are percent (%) occurrence. Mean and x-axis units are in cm/s. Columns represent seasons, rows represent depths. Surface plot x-axes range from -180 to 100 cm/s with a bin size of 10. Subsurface plot x-axes range from -30 to 10 cm/s with a bin size of 1.

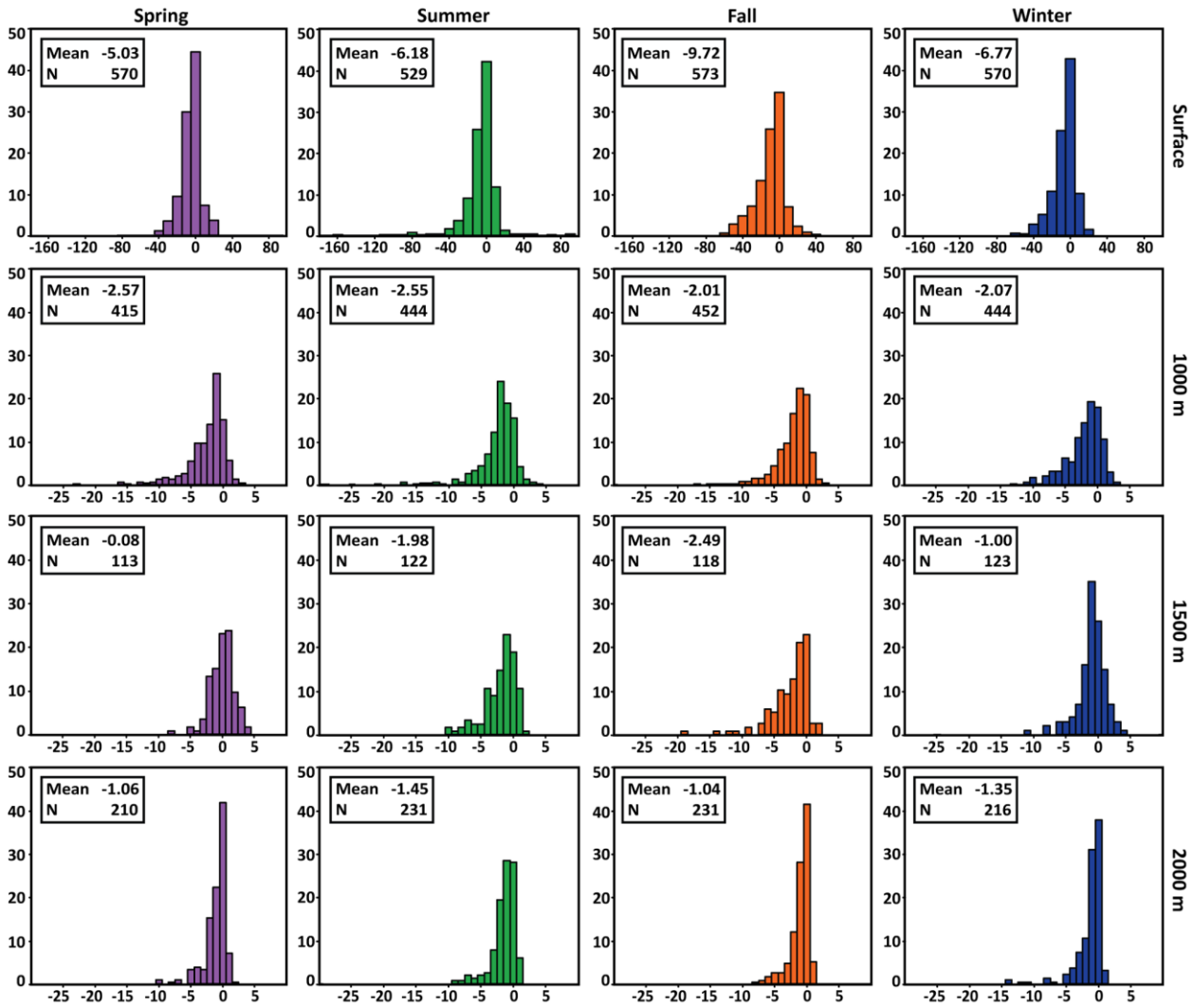
Spring
Summer
Fall
Winter
Surface
1000 m
1500 m
2000 m
Mean -5.03
N 570
Mean -6.18
N 529
Mean -9.72
N 573
Mean -6.77
N 570
Mean -2.57
N 415
Mean -2.55
N 444
Mean -2.01
N 452
Mean -2.07
N 444
Mean -0.08
N 113
Mean -1.98
N 122
Mean -2.49
N 118
Mean -1.00
N 123
Mean -1.06
N 210
Mean -1.45
N 231
Mean -1.04
N 231
Mean -1.35
N 216

Table 1. Data Comparison: Vector correlation, scalar correlation and scalar correlation significance of velocity between SODA output, ARGO floats, and surface drifters.

Velocity Correlation between SODA output and ARGO Float and Surface Drifter Data				
Season	Depth	Vector Correlation	Scalar Correlation	Scalar Correlation Significance (p-value)
Spring	Surface	0.71	0.40	0.00
	1000 m	0.21	0.22	0.20
	1500 m	0.25	0.19	0.40
	2000 m	0.32	0.40	0.52
Summer	Surface	0.93	0.72	0.00
	1000 m	0.10	0.15	0.71
	1500 m	0.24	0.30	0.13
	2000 m	0.18	0.29	0.65
Fall	Surface	0.75	0.54	0.00
	1000 m	0.02	0.17	0.87
	1500 m	0.04	0.12	0.41
	2000 m	0.01	0.22	0.33
Winter	Surface	0.78	0.61	0.00
	1000 m	0.24	0.19	0.60
	1500 m	0.58	0.30	0.32
	2000 m	0.10	0.18	0.47